



Published in final edited form as:

Biomed Pharmacother. 2022 February ; 146: 112459. doi:10.1016/j.biopha.2021.112459.

Discovery of a novel cyclin-dependent kinase 8 inhibitor with an oxindole core for anti-inflammatory treatment

Tony Eight Lin^{a,b,1}, Chia-Ron Yang^{c,1}, Ching-Hsuan Chou^c, Jui-Yi Hsu^{a,d}, Min-Wu Chao^c, Tzu-Ying Sung^e, Jui-Hua Hsieh^f, Wei-Jan Huang^{g,h}, Kai-Cheng Hsu^{a,d,g,i,j,k,*}

^aGraduate Institute of Cancer Biology and Drug Discovery, College of Medical Science and Technology, Taipei Medical University, Taipei, Taiwan

^bMaster Program in Graduate Institute of Cancer Biology and Drug Discovery, College of Medical Science and Technology, Taipei Medical University, Taipei, Taiwan

^cSchool of Pharmacy, College of Medicine, National Taiwan University, Taipei, Taiwan

^dPh.D. Program for Cancer Molecular Biology and Drug Discovery, College of Medical Science and Technology, Taipei Medical University, Taipei, Taiwan

^eBiomedical Translation Research Center, Academia Sinica, Taipei, Taiwan

^fDivision of the National Toxicology Program, National Institute of Environmental Health Sciences, National Institutes of Health, Durham, NC, USA

^gPh.D. Program in Drug Discovery and Development Industry, College of Pharmacy, Taipei Medical University, Taipei, Taiwan

^hGraduate Institute of Pharmacognosy, College of Pharmacy, Taipei Medical University, Taipei, Taiwan

ⁱCancer Center, Wan Fang Hospital, Taipei Medical University, Taipei, Taiwan

^jTMU Research Center of Cancer Translational Medicine, Taipei Medical University, Taipei, Taiwan

^kTMU Research Center of Drug Discovery, Taipei Medical University, Taipei, Taiwan

Abstract

This is an open access article under the CC BY-NC-ND IGO license (<http://creativecommons.org/licenses/by-nc-nd/3.0/igo/>).

*Corresponding author at: Graduate Institute of Cancer Biology and Drug Discovery, College of Medical Science and Technology, Taipei Medical University, Taipei, Taiwan. piki@tmu.edu.tw (K.-C. Hsu).

¹These authors contributed equally to this work.

CRediT authorship contribution statement

Tony Eight Lin: Conceptualization, Methodology, Software, Validation, Formal analysis, Investigation, Writing – original draft and Editing. **Chia-Ron Yang:** Conceptualization, Methodology, Validation, Writing – original draft and Editing. **Ching-Hsuan Chou:** Validation, Formal analysis, Investigation. **Jui-Yi Hsu:** Resources. **Min-Wu Chao:** Validation, Investigation. **Tzu-Ying Sung:** Software, Visualization. **Jui-Hua Hsieh:** Software, Visualization. **Wei-Jan Huang:** Resources. **Kai-Cheng Hsu:** Conceptualization, Methodology, Writing – editing, Supervision, Funding acquisition.

Conflict of interest statement

The authors declare that they have no competing interests.

Appendix A. Supporting information

Supplementary data associated with this article can be found in the online version at doi:10.1016/j.biopha.2021.112459.

Chronic inflammation is an underlying cause in a number of diseases. Cyclin-dependent kinase 8 (CDK8) has been implicated as an inflammatory mediator, indicating its potential as an anti-inflammatory target. Herein, we performed structure-based virtual screening (SBVS) to identify novel CDK8 inhibitors. The pharmacological interactions for CDK8 were identified and incorporated into a SBVS protocol. Selected compounds were tested in enzymatic assays, and one compound was confirmed to be a CDK8 inhibitor with a 50% inhibitory concentration (IC_{50}) value of 1684.4 nM. Comparing structural analogs identified a compound, F059–1017, with greater potency (IC_{50} 558.1 nM). When tested in cell lines, the compounds displayed low cytotoxicity. Cellular assays revealed that the identified CDK8 inhibitors can reduce phosphorylation and expression of signaling mediators associated with inflammation. In addition, results of kinase profiling showed that compound F059–1017 is selective towards CDK8. These findings suggest that the new inhibitors have great potential as lead compounds for developing novel anti-inflammatory therapeutics.

Keywords

Inflammation; CDK8; Kinase inhibitor; Structure-based virtual screening

1. Introduction

Inflammation is a major physiological response that can trigger the immune system to induce signaling for healing, repair, and defense against infection [1,2]. As such, it is tightly regulated by a complex hierarchy of immune cells, receptors, and signal. Aberrant signaling, as well as infection and autoimmune diseases, can lead to chronic inflammation [1–3]. Chronic inflammation is associated with various diseases, including rheumatoid arthritis, asthma, Crohn's disease, and various types of cancer [2–5]. Cancer metastasis and proliferation can also be induced by chronic inflammation [1,6]. This suggests that the inflammatory pathway could be an important target for therapeutics. While anti-inflammatory drugs exist, such as aspirin, non-steroidal anti-inflammatory drugs (NSAIDs), or dexamethasone, their effectiveness may vary depending on the disease and patient [5,7]. As a result, there continues to be a great need for anti-inflammatory therapeutics targeting various medical ailments.

Cyclin-dependent kinases (CDKs) can function as mediators of inflammatory responses [8,9]. The CDK family is comprised of roughly 20 serine-threonine kinases [10,11]. CDKs, along with their regulatory protein cyclins, modify substrates involved in the cell cycle to regulate several extracellular and intracellular responses related to inflammation [10,11]. Expression of the anti-inflammatory cytokine, interleukin (IL)–10, can be regulated by CDK family members [9,12]. Importantly, the activities of pro-inflammatory transcription factors, such as nuclear factor (NF)– κ B, inducible nitric oxide synthase (iNOS) and cyclooxygenase (COX)–2, can be reduced in the absence of CDK enzymatic activity [8,9,12,13]. The potential to target CDKs and their ability to regulate pro-inflammatory signaling make them potential targets for novel anti-inflammatory therapeutics.

Research regarding the CDK8 isozyme revealed that it has specific roles in the innate immune response and inflammation [12,14]. The NF- κ B transcription factor can recruit CDK8, along with its variably expressed paralog, CDK19, to form a complex that is directed toward pro-inflammatory cytokine expression [14]. Furthermore, it was observed that inhibition of CDK8 upregulates the anti-inflammatory IL-10 [12]. Knockout of both CDK8 and CDK19 can decrease chemokine induction [15]. As a result, CDK8 can function as a specific target for modulating the inflammatory or immune response with small molecules. However, the development of potent and selective kinase inhibitors continues to be a persistent challenge. This is due to the highly conserved binding site shared within the kinome. As a result, many kinase inhibitors exhibit off-target side effects. Nevertheless, there has been great success in developing small-molecule kinase inhibitors [16]. Recent research has shown beneficial treatments of rheumatoid arthritis with Janus-associated kinase (JAK) inhibitors [1,17]. Expanding potential targets within inflammatory responses could lead to the identification of novel lead structures and potential therapeutics with greater effectiveness. These trends suggest that a small molecule targeting CDK8 may be a viable candidate for anti-inflammatory therapeutics.

In this study, we performed structure-based virtual screening (SBVS) to identify novel CDK8 inhibitors. A workflow of this study is depicted in Fig. 1. We first identified pharmacological interactions within the CDK8 binding site by analyzing known CDK8 inhibitors. The commercial compound library, ChemDiv, was virtually screened based on the docking score and pharmacological interactions. The top virtual hits were then selected for validation. This workflow led to the identification of a potent CDK8 inhibitor. To better evaluate its CDK8 inhibitory activity and binding mechanism, a series of analogs was analyzed. Surprisingly, one analog was found to have greater CDK8 inhibitory activity. The structure-activity relationship (SAR) was evaluated to better elucidate its potential binding mechanism. When tested *in vitro*, the identified inhibitors showed disruption of the inflammatory pathway. This study revealed a novel inhibitor with potential for further chemical optimization.

2. Methods

2.1. Molecular docking and identification of pharmacological interactions

Compounds were docked using the following molecular docking software: iGEMDOCK [18], CDOCKER module in Discovery Studio [19], SYBYL-X [20], and LeadIT [21] at default settings. The crystal structure (PDB ID: 5HBH) of CDK8 was obtained from Protein Data Bank. The binding site was determined to be 10 Å from the CDK8 co-crystal ligand. The co-crystal ligand (PDB Ligand ID: 5Y7) was redocked into the binding site to evaluate docking performance of the software. The root-mean-square deviation (RMSD) for the respective docking procedures was calculated.

Known CDK8 inhibitors were obtained from the compound database BindingDB. Compounds with an IC₅₀ value of > 10,000 nM were removed. The remaining compounds were clustered using Pipeline Pilot [22], and 30 diverse compounds were selected from the different clusters. The docking performance of software was assessed by mixing 30 known and diverse CDK8 inhibitors with 990 randomly selected compounds from the Available

Chemical Database (ACD) [23]. The compounds were docked and ranked based on the docking scores generated by the docking softwares. The Enrichment factor and Goodness of hit score were calculated to assess the performance of the SBVS used in the study [24].

The docking poses of the 30 known inhibitors generated by LeadIT were then analyzed. Pharmacological interactions in this study were defined as appearing in 50% of the docked CDK8 inhibitors. The pharmacological score was determined as:

$$S(i) = N(i) + (-0.01)D(i)$$

where $S(i)$ is the pharmacological score of compound i , $N(i)$ is the number of pharmacological interactions that compound i forms, and $D(i)$ is the docking score of compound i generated using LeadIT. Compounds with favorable pharmacological scores and availability were selected for further testing.

2.2. Virtual screening

The ChemDiv compound database was selected for screening CDK8 inhibitors. The Pipeline Pilot software was used to filter compounds with structures that matched pan-assay interference compounds (PAINS) [25] and compounds that violated the “Lipinski and Verber Rules”. Finally, the remaining compounds were docked into the CDK8 (PDB ID: 5HBH) crystal structure using LeadIT. The docking protocol used a hybrid approach (enthalpy and entropy). Other docking parameters used default settings. Compounds were ranked based on their pharmacological interactions, and the top-ranked compounds were selected for an assay analysis. Hydrogen-bonding and hydrophobic interactions were analyzed by Pipeline Pilot.

2.3. Kinase assay

Kinase assays were performed in cell-free, *in vitro* assays using the ThermoFisher Scientific SelectScreen kinase profiling service (www.thermofisher.com/selectscreen). Both the LanthaScreen and Z'-LYTE technology were used in evaluating kinase activity. In brief, test compounds were co-incubated with a fluorescent-labeled substrate, kinase, ATP, kinase buffer, and development for reaction for 1 h before the stop solution, EDTA, was added. Results were determined using a fluorescence reader. The reported result is an average of two replicates.

2.4. Cell culture

Murine RAW264.7 cells, a mouse macrophage cell line, were obtained from the Bioresource Collection and Research Center (BCRC; Hsinchu City, Taiwan). Mouse BV-2 microglia and the human HEK-293 embryonic kidney epithelial cell line were kindly provided by Prof. Shiow-Lin Pan (Graduate Institute of Cancer Biology and Drug Discovery, Taipei Medical University, Taipei, Taiwan). RAW264.7 and BV-2 cells were cultured in Dulbecco's modified Eagle medium (DMEM; Invitrogen Life Technologies, Carlsbad, CA, USA) supplemented with 10% (vol/vol) fetal bovine serum (FBS; Invitrogen Life Technologies, Carlsbad, CA, USA), 100 U/mL penicillin, and 100 µg/mL streptomycin (Biological Industries, Kibbutz Beit Haemek, Israel). HEK-293 cells were maintained in minimum essential medium (MEM) with 10% FBS, 1 mM sodium pyruvate, penicillin (100 U/mL),

and streptomycin (100 µg/mL). Cells were incubated at 37 °C in a humidified atmosphere of 5% CO₂ in air.

2.5. Cell cytotoxicity assay

Cell cytotoxicity was measured by a colorimetric 3-(4,5-dimethylthiazol-2-yl)-2,5-diphenyltetrazolium bromide (MTT) assay. Cells (10⁴) in 1 mL of medium in 96-well plates were incubated with the vehicle (control) or the vehicle with a test compound for 48 h. After various treatments, 1 mg/mL of MTT was added, and plates were incubated at 37 °C for an additional 2 h; then, cells were pelleted and lysed by DMSO, and the absorbance at 570 nm was measured on a microplate reader.

2.6. RNA extraction and real-time PCR

Total RNA was isolated using a TRIzol and Direct-zol™ RNA Mini-Prep kit (ZYMO Research, Irvine, CA, USA) following the manufacturer's instructions. Reverse-transcription to cDNA was performed using a random primer and M-MLRT. In brief, first-strand cDNA was synthesized using 1 µg of mRNA incubated with a random primer at 65 °C for 5 min and then reacted with M-MLRT at 37 °C for 1 h. For the real-time PCR, cDNAs were amplified in SYBR Green PCR Master Mix (Life Technologies, Grand Island, NY, USA) and detected with the Applied Biosystems StepOnePlus™ Q-PCR detection system. Relative gene expression was normalized to GAPDH and calculated using the 2^(-CT) method.

2.7. Immunoblot analyses

Cells (1 × 10⁶) were incubated for 10 min at 4 °C in lysis buffer (20 mM HEPES at pH 7.4, 2 mM EGTA, 50 mM β-glycerophosphate, 0.1% Triton X-100, 10% glycerol, 1 mM DTT, 1 µg/mL of leupeptin, 5 µg/mL of aprotinin, 1 mM phenylmethylsulfonyl fluoride, and 1 mM sodium orthovanadate), scraped off, incubated on ice for an additional 10 min, and centrifuged at 17,000 *g* for 30 min at 4 °C. Protein samples (20 µg) were then electrophoresed on sodium dodecyl sulfate polyacrylamide gel electrophoresis (SDS-PAGE) gels and transferred to a nitrocellulose membrane, which was then blocked by incubation for 30 min at room temperature with 5% bovine serum albumin (BSA) in Tris-buffered saline with 0.1% Tween-20 (TBST). Immunoblotting was performed by overnight incubation at 4 °C with primary antibodies in TBST, followed by incubation for 1 h at room temperature with horseradish peroxidase (HRP)-conjugated secondary antibodies. Bound antibodies were measured using an enhanced chemiluminescence (ECL) reagent (GE Healthcare, Buckinghamshire, UK) and exposed to photographic film. The antibody used in this study as follows: p-p65, p-IκBα, iNOS and β-actin were purchased from Abclonal Inc., (Woburn, MA, USA); p65 was purchased from Biovision Inc. (Mountain View, CA, USA); IκBα was purchased from Santa Cruz Biotechnology Inc. (Dallas, Texas, USA); COX-2 was purchased from Epitomics Inc. (Burlingame, California, USA); α-tubulin was purchased from Genetex Inc. (Hsinchu City, Taiwan, ROC).

2.8. Nitrate assay

Nitrite production was measured in RAW264.7 macrophage and BV-2 microglia cell supernatants. Briefly, cells (10⁶) were cultured in six-well plates and stimulated

with lipopolysaccharide (LPS; 100 ng/mL; Sigma-Aldrich Pty Ltd., KGaA, Darmstadt, Germany) for 24 h, then 100 μ L of Griess reagent (1% sulphanilamide and 0.1% naphthylethylenediamide in 5% phosphoric acid) was mixed with 100 μ L of the cell supernatant, and the optical density at 550 nm was measured. The concentration of nitrite was calculated from a standard curve prepared using known concentrations of sodium nitrite dissolved in DMEM.

2.9. SAR modeling and analysis

The molecular force fields were generated using the molecular program Forge [26]. This program generates a 3D map that displays activity cliffs that reveal favorable and unfavorable electrostatic and hydrophobic fields between a protein and compounds. The activity cliffs represent compound pairs with structural differences that can lead to great differences in potency. The molecular field for each compound was generated. Then, the compounds were aligned to the docking pose of the most potent inhibitor. The model was created using default settings.

The Comparative Molecular Field Analysis (CoMFA) models were generated using SYBYL-X [20]. Compounds were aligned based on their scaffold, and their biological activities were included in a molecular spreadsheet. Hydrogen atoms were added, and charges were assigned Gasteiger-Huckel charges. The inhibition percentages were used as activity data in CoMFA analysis. The inhibition percentages [27] were converted using the following:

$$\log - (P/100 - P)$$

where P is the inhibition percentage at 10 μ M concentration. Default settings were used to calculate steric and electrostatic fields around the aligned molecules. The partial least square (PLS) method with leave-one-out cross validation was used to determine the optimum number of components. Finally, the CoMFA results were represented as a 3D model with field contour maps.

2.10. Compound similarity score

The structure of the identified inhibitor was compared to those of 30 known CDK8 inhibitors. An atom-pair fingerprint of each compound was generated using RDKit Fingerprint tool in KNIME [28]. A similarity score was produced for each compound using Pearson correlation coefficient. A score of 1–0 denotes compounds most similar to least similar, respectively, to the identified inhibitor.

2.11. Data analysis and statistics

Data are expressed as the mean \pm standard error of the mean (SEM) and were analyzed using a one-way analysis of variance (ANOVA). When the ANOVA showed a significant difference between groups, Tukey's *post-hoc* test was used to determine the pairs of groups showing statistically significant differences. Parameters with $p < 0.05$ were considered statistically significant.

3. Results and discussion

3.1. Establishing pharmacological interactions

The workflow of this study is depicted in Fig. 1. Structural information from the target protein can be used to identify important protein-ligand interactions [29]. Analyzing docking poses of known CDK8 inhibitors may also reveal pharmacological interactions that can be used as one of the filtering criteria [18, 30]. Typically, the kinase ATP binding site is situated between the N-lobe and C-lobe. The former consists of a β -sheet, while the latter features α -helices and loops. Both lobes are connected by a hinge motif [31]. The adenine ring of ATP forms hydrogen bonds with hinge residues. These hydrogen bond interactions with hinge residues are a common feature of many small-molecule inhibitors that occupy the ATP binding site [32]. Understanding these features is an important step in developing a virtual screening protocol and can lead to designs of novel inhibitors with greater affinity or selectivity.

The docking protocol in this study was first validated by re-docking the co-crystal ligand (PDB Ligand ID: 5Y7) of CDK8 (PDB ID: 5HBH). This procedure ensured that the docking program could accurately reproduce the pose of the co-crystal structure [33]. Four molecular docking programs were tested to determine the most favorable docking protocol for use in the study: iGEMDOCK [18], the CDOCKER package found in Discovery Studio [19], SYBYL-X [20], and LeadIT [21]. Superimposing the docking pose of the co-crystal ligand showed that a favorable docking protocol was used for this study with LeadIT or CDOCKER, which produced an RMSD score of 1.13 Å and 0.81 Å, respectively (Supplementary Fig. 1). We next tested their docking performance. A total of 30 known CDK8 inhibitors were mixed 990 compounds randomly selected from the ACD [23]. Compounds were docked using LeadIT or CDOCKER. Overall, compounds docked with LeadIT were ranked higher than that of CDOCKER (Supplementary Fig. 2). These results suggest that LeadIT would offer greater docking performance for identifying potential CDK8 inhibitors in this study.

Pharmacological interactions can also facilitate our understanding of the protein-ligand interactions. To that end, we sought to identify pharmacological interactions within the CDK8 binding site [18]. Known CDK8 inhibitors were obtained from BindingDB [34]. In total, 30 CDK8 inhibitors with diverse structures were docked into the target protein using LeadIT [21]. An analysis of their docking poses identified three ATP binding site residues that formed hydrogen bonds at a frequency of 50% with known CDK8 inhibitors (Fig. 2). Residues D98 and A100 are part of the hinge loop, and hydrogen bonds respectively occurred with at least 90% and 60% of known CDK8 inhibitors. Analyzing docking poses of known CDK8 inhibitors showed a hydrogen bond with at least one hinge residue (Supplementary Fig. 3). While a hydrogen bond with the hinge residue is necessary, increasing the number does not necessarily lead to increased potency [35]. This suggests that a hydrogen bond with either D98 or A100 was necessary for CDK8 inhibition. At a frequency 50%, residue K52 was observed to form the final favorable hydrogen bond within the CDK8 binding site. Residue K52 plays a key role in CDK8 activity by forming a salt bridge with residue E66, which stabilizes the active conformation of CDK8 [36].

Disruption of the salt bridge may be beneficial for inhibiting the enzymatic activity of CDK8. Interestingly, when ATP was docked into the CDK8 binding site, hydrogen bonds formed with the three aforementioned residues (Fig. 2B). Thus, residues A100, D98, and K52 may be important pharmacological interactions for CDK8 inhibition.

Five hydrophobic pharmacological interactions were also identified (Fig. 2A). Hydrophobic interactions can support or coordinate with the adenine ring of ATP [37]. The hydrocarbon side chains of V158 and V35 and the methyl side chain of A50 form a hydrophobic pocket that sandwiches the adenine scaffold of ATP (Fig. 2B). Hinge residue A100 also contributes to favorable hydrophobic interactions due to its methyl side chain. Residue Y99 contains a large phenol ring that is able to form an offset π - π stacking interaction with the ATP adenine scaffold. Known CDK8 inhibitors contain heterocyclic scaffolds that can occupy the adenine pocket and may form hydrophobic interactions with the aforementioned residues (Supplementary Fig. 3). The identified pharmacological interactions may reveal potential inhibitors within the CDK8 binding site.

3.2. Virtual screening and validation of CDK8 inhibitory activity

To determine the screening performance of the protocol used in this study, we mixed 30 known CDK8 inhibitors with 990 compounds randomly selected from the ACD and docked them into CDK8. The compounds were then ranked by their docking score alone or by pharmacological interactions. The rank of true hit compounds, or the percentage of known CDK8 inhibitors, was higher when using pharmacological interactions (Supplementary Fig. 4A). The Enrichment Factor and Goodness of hit were generated at 10%, 20%, and 30%. We found that for our study, ranking compounds using pharmacological interactions produced more favorable values compared to docking score alone (Supplementary Fig. 4B–C). A ROC curve for pharmacological and docking scoring strategies further illustrates their scoring differences (Supplementary Fig. 4D).

Compounds from the ChemDiv library (~1.6 million compounds) were virtually screened for potential CDK8 inhibitors. The library was first prepared using pre-filtering rules. These rules are a method of evaluating drug-likeness of a compound and are a good indicator for potential small-molecule inhibitors [38]. Compounds that contain PAINS structures and possess a calculated quantitative estimate of drug-likeness (QED) score of > 0.25 were removed [25,38]. Many kinase inhibitors contain a heterocyclic ring consisting of hydrogen bond donors and acceptors that mimic interactions observed between adenine and the kinase hinge [32]. Therefore, compounds that do not contain a heterocyclic ring system were removed. The remaining compounds were docked and then ranked based on their docking score, with the top 10,000 compounds selected. These compounds were then re-ranked based on the sum of their pharmacological interactions. The top 40 compounds were then visually inspected, and 13 compounds were selected for further study. The 13 compounds were tested at 10 μ M using the ThermoFisher SelectScreen kinase profiling service. The assay revealed a hit, compound E966–0578, with CDK8 inhibitory activity of 83% at 10 μ M (Table 1). Thus, we identified a potential CDK8 inhibitor using an SBVS approach.

To elucidate the binding mechanism of compound E966–0578, we sourced its analogs within the ChemDiv library. In total, 22 analogs were selected for analysis. The analogs

shared an oxindole scaffold with a sulfonamide at the 5-position (Table 2). However, a nitrogen was substituted on the 3-position of compound G801–0002. The analogs were tested for CDK8 inhibitory activity as mentioned above. Surprisingly, three analogs were found to inhibit CDK8 with percentages of 83% (Table 2). The most potent compound, F059–1017, not only had an inhibitory activity of 93% towards CDK8, but also an IC_{50} value of 558.1 nM (Table 3). This is in stark contrast to the hit compound E966–0578 (IC_{50} 1684.4 nM) and the analog E966–0445 (IC_{50} 2573 nM). Both compounds inhibited CDK8 activity by 83% (Table 2). This suggests the oxindole can serve as a suitable CDK8 inhibitor and that differences in potency may be due to substituents on the core oxindole kinase scaffold (Table 1).

The docking pose of compound F059–1017 showed favorable occupation of the CDK8 binding site (Fig. 3). The oxindole ring of compound F059–1017 occupied the adenine position of the CDK8 binding site. The oxindole ring contains a nitrogen and a carbonyl oxygen that facilitated hydrogen bond to hinge residues D98 and A100, respectively (Fig. 3). An additional hydrogen-bond interaction was formed with the sulfonamide functional group and K52 residue. Importantly, these three hydrogen bonds were identified as pharmacological interactions (Fig. 2). The oxindole also formed hydrophobic interactions with residues A50, A100, and L158. The cyclopentane moiety attached to the oxindole 3-position formed hydrophobic interactions with residues V27 and V35. The benzene functional group, which is attached to the sulfonamide, occupied another pocket to form hydrophobic interactions with residue Y32. Together, these interactions suggested that compound F059–1017 was favorably positioned within the CDK8 binding site.

3.3. SAR analysis of compound F059–1017 and analogs

To better understand binding interactions of F059–1017, a SAR analysis was performed. A model was created using the molecular software, Forge [26]. The model displayed activity cliffs, which are identified by groups of structurally similar compounds with activity against the same target, but contain great differences in potency [39]. Activity cliffs summarize favorable and unfavorable regions, such as sites of hydrophobic or electrostatic interactions, between the indicated group of compounds. Compound F059–1017 occupied two favorable hydrophobic regions (Fig. 4A). One region was occupied by the cyclopentane moiety of compound F059–1017. In contrast, the analogs F966–0602 and G801–0002 contained an isobutylene and a lone hydrogen atom, respectively. As a result, these analogs were unable to favorably occupy the hydrophobic pocket (Fig. 4B). The benzene moiety of F059–1017 occupied a second favorable hydrophobic pocket. Analogs E966–0482 and F059–0343 respectively contained a 1,4-xylene and 1, 3-xylene moiety. These bulky moieties contained a one-carbon chain attached to a sulfonamide which added flexibility to their structure. These analogs favored a binding pose that did not extend into this favorable hydrophobic pocket (Fig. 4C). Adjacent to this favorable hydrophobic pocket was an unfavorable hydrophobic pocket (Fig. 4D). The analogs F966–0439, F059–0151, and F966–0486 contained further substitutes on their benzene ring that extended into this unfavorable hydrophobic pocket (Fig. 4D). The CDK8 binding site contained a negative electrostatic site. The sulfamide of compound F059–1017 was positioned in a favorable position to occupy the negative electrostatic site. This was due to the position of the oxygen located

on the sulfamide (Fig. 4A). In contrast, the sulfamide of analog F966–0482 was positioned away from this site and was unable to form negative electrostatic interactions (Fig. 4E). CDK8 also contains areas of positive electrostatic sites, which favor hydrogen donating moieties (Fig. 4F). The acetamide moiety of analog F966–0578 occupied this site and may have reduced its effectiveness towards CDK8 inhibition. The inactive analog F966–0467 contained a two-carbon chain that extended into this site; however, the carbon chain did not function as a hydrogen donor. Together, the SAR analysis identified favorable characteristics of the active analog F059–1017 within the CDK8 binding site.

To further confirm the SAR analysis above, we created a CoMFA model using SYBYL-X [20]. The analogs with the same scaffold were aligned to F059–1017, and molecular fields were calculated [40]. The CoMFA molecular fields correspond to steric or electrostatic properties. The results of the CoMFA model are summarized in Supplementary Table 1. The PLS method with leave-one-out option was used to identify the cross-validated q^2 value of 0.701. The non-cross validated PLS analysis showed conventional r^2 value of 0.988. The standard error of the estimate was found to be 0.075. The steric models contribute to 80.5% of the CoMFA model, while electrostatics amounted to 19.5%. The 3D model with compound F059–1017 can be observed in Supplementary Fig. 5. The green contours represent regions with bulky groups. These may confer increased inhibition potency. For example, F059–1017 contains a cyclopentane and a benzene moiety that corresponds to the favorable steric regions. In comparison, F966–0602 contains an isobutylene that does not occupy the favorable steric regions. Compound F966–0486 contains additional substituents on the benzene moiety, which would extend the compound into an unfavorable steric pocket (yellow contour region). The red contours represent regions with desirable electronegative moieties. F059–1017 does not extend into this region. This suggests possible avenues to optimize potency towards CDK8. In general, the CoMFA studies support the activity cliffs identified in Forge (Fig. 4).

3.4. In vitro evaluations of selected compounds reveal the ability to modulate inflammatory pathways

To evaluate the effects of the compounds on cell viability, the compounds were tested *in vitro*. The compounds selected for testing, E966–0482, F069–0210, and F059–1017, were shown to have a varying range of CDK8 inhibitory activities at 10 μ M of 15%, 44%, and 96%, respectively (Table 2). The compounds were tested in RAW264.7 macrophages, BV-2 microglia, and HEK293 cells. Cell viabilities in treated cells did not significantly change when treated with these compounds for 12, 24, and 48 h (Fig. 5). This was also observed when compound concentrations were increased up to 20 μ M. This suggests that the compounds did not cause cell toxicity at the tested concentrations.

It was reported that CDK8/19 can affect NF- κ B activation [14]. The CDK8/19 complex is recruited to NF- κ B-responsive promoters and phosphorylates the C-terminal domain of RNA polymerase II, which then initiates NF- κ B transcription and triggers expressions of pro-inflammatory cytokines [14]. The identified CDK8 inhibitors were further examined for modulation of NF- κ B expression. BV2 and RAW264.7 cells were treated with LPS to induce phosphorylation of p65, a component of the NF- κ B transcription factor family

[41]. The potent glucocorticoid steroid, dexamethasone, was shown to interfere with NF- κ B activation and was used as a positive control [42]. Compound F059–0210 displayed a slight reduction in RAW264.7 cells, while E966–0482 displayed no significant reduction in phosphorylated P65 expression (Fig. 6A–B). This appears consistent with their CDK8 inhibitory activities observed previously (Table 2). In contrast, a significant reduction in phosphorylated P65 expression in both cell lines was observed when treated with compound F059–1017 (Fig. 6A–B). Of the compounds tested, F059–1017 displayed the greatest potency.

Modulation of downstream NF- κ B signaling was further evaluated when treated with the identified CDK8 inhibitors. Downstream inflammatory factors of NF- κ B include COX-2 and iNOS [43]. To evaluate if F059–1017 or F059–0210 can modulate inflammatory signaling at a lower concentration (3 μ M) compared to the weaker CDK8 inhibitor E966–0482 at 10 μ M. Compound F059–1017 exhibited potent inhibition of COX-2 and iNOS expressions in LPS-treated cells when its concentration was reduced to 3 μ M (Fig. 7). By contrast, the mild and moderate CDK8 inhibitors (*e.g.*, 10 μ M of E966–0482 and 3 μ M of F059–0210) displayed less inhibition of inflammatory factors. This suggests F059–1017 to be a more potent modulator of inflammatory signaling. Several upstream mediators can induce NF- κ B activity. One such example is inhibitor protein I κ B α . When cells are exposed to LPS, I κ B α is phosphorylated by I κ B kinase (IKK) and degraded, which triggers NF- κ B signaling [44]. The CDK8 inhibitor F059–1017 showed no significant effect in increasing LPS-induced expression of phosphorylated I κ B α (Supplementary Fig. 6A). Tumor necrosis factor (TNF)- α is a pro-inflammatory cytokine that can also induce NF- κ B [14]. Cells treated with TNF- α showed an increase in phosphorylated p65 expression, which suggests activation of NF- κ B (Fig. 8A). Genes coregulated with NF- κ B include C-X-C motif chemokine ligand 1 (CXCL1) and IL-8 [14]. Both CXCL1 and IL-8 belong to a cytokine family and are critical inflammatory mediators [45]. Treatment with TNF- α increased both cytokine mRNA expression levels (Fig. 8B). However, treatment with F059–1017 reduced production of TNF- α -induced inflammatory factors. The mRNA expression of pro-inflammatory mediators TNF- α and IL-1 β was found to be reduced when treated with F059–1017 in cells exposed to LPS (Supplementary Fig. 6B–C). A potent CDK8 inhibitor, Senexin A, was reported to perturb TNF- α signaling [14]. In contrast, the identified inhibitors, E966–0482 and F059–0210, produced less potent inhibition of IL-8 and CXCL1 expressions (Fig. 8B). These inhibitors did not produce a significant effect to the mRNA expression of TNF- α and IL-1 β in LPS treated cells. Together, these results suggested that F059–1017 is the potent CDK8 inhibitor and can potentially modulate signaling pathways associated with the inflammatory response.

3.5. Compound F059–1017 shows selectivity towards CDK8 and has a novel structure

The goal of this study was to identify novel and selective CDK8 inhibitors. The conserved nature of the kinome has proven a challenge in developing selective and potent small-molecule inhibitors [16]. Many CDK inhibitors are non-selective and may target other related CMGC kinase members [46]. As a signaling mediator, CDK8 is involved with regulating transcription of many different cell types that may induce cytotoxic effects [11]. Further, a more selective inhibitor may reduce potential side effects when targeting CDK8

[14]. To assess the selectivity of F059–1017, we used the commercially available kinase profiling platform by ThermoFisher against a panel of kinases in the CMGC family. The profiling results showed that compound F059–1017 exhibited inhibition percentages of 32% and 33% for the closely related kinases, CDK2 and CDK3, respectively. The next most potent inhibition occurred with CDK19, which is a paralog of CDK8 (Supplementary Table 2). These results suggest that F059–1017 has greater selectivity towards CDK8.

To determine the novelty of the F059–1017 structure, we compared its structure to known CDK8 inhibitors. A similarity score was obtained using the Pearson correlation coefficient. The similarity score ranges 0–1, with 1 being the most similar. Compound F059–1017 was compared to 30 diverse CDK8 inhibitors used to generate pharmacological interactions. In general, the known inhibitors generated a similarity score of <0.3, suggesting that compound F059–1017 has a novel structure (Supplementary Fig. 7). Inhibitors CHEMBL2002649 and CHEMBL1990885 possessed the most similar structures with respective similarity scores of 0.29 and 0.24. These compounds greatly differ with their substituents along the core scaffold. Together, these results suggest that compound F059–1017 is a CDK8 inhibitor with a novel scaffold.

4. Conclusions

CDK8 is a member of the CDK family of serine-threonine protein kinases. Its aberrant expression is associated with inflammation, making it an anti-inflammatory target [12,14]. In this study, we employed an SBVS approach to identify CDK8 inhibitors. Pharmacological interactions of the CDK8 binding site were identified to increase the potential of identifying a hit compound. The screening protocol led to identification of compound E966–0578 (with an IC_{50} of 1684.4 nM). Analogs were obtained to further elucidate the binding mechanism. Interestingly, one analog, F059–1017, was found to have greater CDK8 inhibitory activity (with an IC_{50} of 558.1 nM). When tested *in vitro*, these compounds showed an ability to reduce expressions of pro-inflammatory mediators, such as IL-8. Inflammation can also result from pro-inflammatory cytokines released by tumors. It may be possible that targeting CDK8 may not only have an anti-inflammatory effect, but also an anticancer effect [12,14]. The CDK8 inhibitor identified in this paper can function as an important lead compound for further research.

Supplementary Material

Refer to Web version on PubMed Central for supplementary material.

Acknowledgments

We gratefully acknowledge the support from the Ministry of Science and Technology (MOST 108-2320-B-038-058-MY3 and MOST 109-2320-B-002-049-MY3). This research was also partially supported by Biomedical Translation Research Center, Academia Sinica (Grant No. AS-BRPT-110-06), Health and welfare surcharge of tobacco products (MOHW110-TDU-B-212-144020) and "TMU Research Center of Cancer Translational Medicine" from the Higher Education Sprout Project by the Ministry of Education (MOE) in Taiwan.

References

- [1]. Zarrin AA, Bao K, Lupardus P, Vucic D, Kinase inhibition in autoimmunity and inflammation, *Nat. Rev. Drug Disco* (2020).
- [2]. Greten FR, Grivennikov SI, Inflammation and cancer: triggers, mechanisms, and consequences, *Immunity* 51 (1) (2019) 27–41. [PubMed: 31315034]
- [3]. Marks DJ, Harbord MW, MacAllister R, Rahman FZ, Young J, Al-Lazikani B, Lees W, Novelli M, Bloom S, Segal AW, Defective acute inflammation in Crohn's disease: a clinical investigation, *Lancet* 367 (9511) (2006) 668–678. [PubMed: 16503465]
- [4]. Murdoch JR, Lloyd CM, Chronic inflammation and asthma, *Mutat. Res.* 690 (1–2) (2010) 24–39. [PubMed: 19769993]
- [5]. Radawski C, Genovese MC, Hauber B, Nowell WB, Hollis K, Gaich CL, DeLozier AM, Gavigan K, Reynolds M, Cardoso A, Curtis JR, Patient perceptions of unmet medical need in rheumatoid arthritis: a cross-sectional survey in the USA, *Rheuma Ther* 6 (3) (2019) 461–471.
- [6]. Han Y, Guo W, Ren T, Huang Y, Wang S, Liu K, Zheng B, Yang K, Zhang H, Liang X, Tumor-associated macrophages promote lung metastasis and induce epithelial-mesenchymal transition in osteosarcoma by activating the COX-2/STAT3 axis, *Cancer Lett* 440–441 (2019) 116–125.
- [7]. Brune K, Patrignani P, New insights into the use of currently available non-steroidal anti-inflammatory drugs, *J. Pain. Res* 8 (2015) 105–118. [PubMed: 25759598]
- [8]. Schmitz ML, Kracht M, Cyclin-dependent kinases as coregulators of inflammatory gene expression, *Trends Pharm. Sci* 37 (2) (2016) 101–113. [PubMed: 26719217]
- [9]. Pfander P, Fidan M, Burret U, Lipinski L, Vettorazzi S, Cdk5 deletion enhances the anti-inflammatory potential of gc-mediated gr activation during inflammation, *Front Immunol* 10 (2019) 1554. [PubMed: 31354714]
- [10]. Kalra S, Joshi G, Munshi A, Kumar R, Structural insights of cyclin dependent kinases: implications in design of selective inhibitors, *Eur. J. Med Chem* 142 (2017) 424–458. [PubMed: 28911822]
- [11]. Xi M, Chen T, Wu C, Gao X, Wu Y, Luo X, Du K, Yu L, Cai T, Shen R, Sun H, CDK8 as a therapeutic target for cancers and recent developments in discovery of CDK8 inhibitors, *Eur. J. Med Chem* 164 (2019) 77–91. [PubMed: 30594029]
- [12]. Johannessen L, Sundberg TB, O'Connell DJ, Kolde R, Berstler J, Billings KJ, Khor B, Seashore-Ludlow B, Fassel A, Russell CN, Latorre IJ, Jiang B, Graham DB, Perez JR, Sicinski P, Phillips AJ, Schreiber SL, Gray NS, Shamji AF, Xavier RJ, Small-molecule studies identify CDK8 as a regulator of IL-10 in myeloid cells, *Nat. Chem. Biol* 13 (10) (2017) 1102–1108. [PubMed: 28805801]
- [13]. Xiang Z, Ho L, Valdellon J, Borchelt D, Kelley K, Spielman L, Aisen PS, Pasinetti GM, Cyclo-oxygenase (COX)-2 and cell cycle activity in a transgenic mouse model of Alzheimer's disease neuropathology, *Neurobiol. Aging* 23 (3) (2002) 327–334. [PubMed: 11959394]
- [14]. Chen M, Liang J, Ji H, Yang Z, Altilla S, Hu B, Schronce A, McDermott MSJ, Schools GP, Lim CU, Oliver D, Shtutman MS, Lu T, Stark GR, Porter DC, Broude EV, Roninson IB, CDK8/19 Mediator kinases potentiate induction of transcription by NFkappaB, *Proc. Natl. Acad. Sci. USA* 114 (38) (2017) 10208–10213. [PubMed: 28855340]
- [15]. Li J, Ji H, Porter DC, Broude EV, Roninson IB, Chen M, Characterizing CDK8/ 19 Inhibitors through a NFkappaB-Dependent Cell-Based Assay, *Cells* 8 (10) (2019).
- [16]. Roskoski R Jr., Properties of FDA-approved small molecule protein kinase inhibitors: A 2020 update, *Pharm. Res* 152 (2020), 104609.
- [17]. Roskoski R Jr., Janus kinase (JAK) inhibitors in the treatment of inflammatory and neoplastic diseases, *Pharm. Res* 111 (2016) 784–803.
- [18]. Hsu KC, Chen YF, Lin SR, Yang JM, iGEMDOCK: a graphical environment of enhancing GEMDOCK using pharmacological interactions and post-screening analysis, *BMC Bioinforma* 12 (Suppl 1) (2011) S33.
- [19]. Wu G, Robertson DH, Brooks CL 3rd, Vieth M, Detailed analysis of grid-based molecular docking: a case study of CDOCKER-A CHARMM-based MD docking algorithm, *J. Comput. Chem* 24 (13) (2003) 1549–1562. [PubMed: 12925999]

- [20]. Sybyl-X Molecular Modeling Software Packages, Version 2.0, 2012.
- [21]. LeadIT v2.3.2, BiosolveIT GmbH, Sankt Augustin, Germany, Available from: <<http://www.biosolveit.de/LeadIT>>.
- [22]. Dassault Systèmes BIOVIA, BIOVIA Pipeline Pilot, Dassault Systemes, release 2017.
- [23]. Bissantz C, Folkers G, Rognan D, Protein-based virtual screening of chemical databases. 1. Evaluation of different docking/scoring combinations, *J. Med Chem* 43 (25) (2000) 4759–4767. [PubMed: 11123984]
- [24]. Niu M, Wang F, Li F, Dong Y, Gu Y, Establishment of a screening protocol for identification of aminopeptidase N inhibitors, *J. Taiwan Inst. Chem. Eng* 49 (2015) 19–26. [PubMed: 32336998]
- [25]. Baell JB, Nissink JWM, Seven year itch: pan-assay interference compounds (PAINS) in 2017-utility and limitations, *ACS Chem. Biol* 13 (1) (2018) 36–44. [PubMed: 29202222]
- [26]. Cheeseright T, Mackey M, Rose S, Vinter A, Molecular field extrema as descriptors of biological activity: definition and validation, *J. Chem. Inf. Model* 46 (2) (2006) 665–676. [PubMed: 16562997]
- [27]. Pandey G, Saxena AK, 3D QSAR studies on protein tyrosine phosphatase 1B inhibitors: comparison of the quality and predictivity among 3D QSAR models obtained from different conformer-based alignments, *J. Chem. Inf. Model* 46 (6) (2006) 2579–2590. [PubMed: 17125198]
- [28]. Berthold MR, Cebron N, Dill F, Gabriel TR, Kötter T, Meinel T, Ohl P, Sieb C, Thiel K, Wiswedel B, KNIME: the Konstanz Information Miner, Springer Berlin Heidelberg, Berlin, Heidelberg, 2008, pp. 319–326.
- [29]. Lionta E, Spyrou G, Vassilatis DK, Cournia Z, Structure-based virtual screening for drug discovery: principles, applications and recent advances, *Curr. Top. Med Chem* 14 (16) (2014) 1923–1938. [PubMed: 25262799]
- [30]. Lin TE, HuangFu WC, Chao MW, Sung TY, Chang CD, Chen YY, Hsieh JH, Tu HJ, Huang HL, Pan SL, Hsu KC, A novel selective JAK2 inhibitor identified using pharmacological interactions, *Front Pharm* 9 (2018) 1379.
- [31]. McClendon CL, Kornev AP, Gilson MK, Taylor SS, Dynamic architecture of a protein kinase, *Proc. Natl. Acad. Sci. USA* 111 (43) (2014) E4623–E4631. [PubMed: 25319261]
- [32]. Derewenda ZS, Hawro I, Derewenda U, C horizontal line Hcdots, three dots, centeredO hydrogen bonds in kinase-inhibitor interfaces, *IUBMB Life* 72 (6) (2020) 1233–1242. [PubMed: 32271995]
- [33]. Hevener KE, Zhao W, Ball DM, Babaoglu K, Qi J, White SW, Lee RE, Validation of molecular docking programs for virtual screening against dihydropteroate synthase, *J. Chem. Inf. Model* 49 (2) (2009) 444–460. [PubMed: 19434845]
- [34]. Liu T, Lin Y, Wen X, Jorissen RN, Gilson MK, BindingDB: a web-accessible database of experimentally determined protein-ligand binding affinities, *Nucleic Acids Res* 35(Database Issue) (2007) D198–D201. [PubMed: 17145705]
- [35]. Xing L, Klug-Mcleod J, Rai B, Lunney EA, Kinase hinge binding scaffolds and their hydrogen bond patterns, *Bioorg. Med Chem* 23 (19) (2015) 6520–6527. [PubMed: 26358279]
- [36]. Wang T, Yang Z, Zhang Y, Yan W, Wang F, He L, Zhou Y, Chen L, Discovery of novel CDK8 inhibitors using multiple crystal structures in docking-based virtual screening, *Eur. J. Med Chem* 129 (2017) 275–286. [PubMed: 28231524]
- [37]. Kornev AP, Taylor SS, Ten Eyck LF, A helix scaffold for the assembly of active protein kinases, *Proc. Natl. Acad. Sci. USA* 105 (38) (2008) 14377–14382. [PubMed: 18787129]
- [38]. Bickerton GR, Paolini GV, Besnard J, Muresan S, Hopkins AL, Quantifying the chemical beauty of drugs, *Nat. Chem* 4 (2) (2012) 90–98. [PubMed: 22270643]
- [39]. Hu Y, Stumpfe D, Bajorath J, Advancing the activity cliff concept, *F1000 Res* 2 (2013) 199.
- [40]. Cramer RD, Patterson DE, Bunce JD, Comparative molecular field analysis (CoMFA). 1. Effect of shape on binding of steroids to carrier proteins, *J. Am. Chem. Soc* 110 (18) (1988) 5959–5967. [PubMed: 22148765]
- [41]. Giridharan S, Srinivasan M, Mechanisms of NF-kappaB p65 and strategies for therapeutic manipulation, *J. Inflamm. Res* 11 (2018) 407–419. [PubMed: 30464573]

- [42]. Crinelli R, Antonelli A, Bianchi M, Gentilini L, Scaramucci S, Magnani M, Selective inhibition of NF- κ B activation and TNF- α production in macrophages by red blood cell-mediated delivery of dexamethasone, *Blood Cells Mol. Dis* 26 (3) (2000) 211–222. [PubMed: 10950941]
- [43]. Tak PP, Firestein GS, NF- κ B: a key role in inflammatory diseases, *J. Clin. Invest* 107 (1) (2001) 7–11. [PubMed: 11134171]
- [44]. McKenna S, Butler B, Jatana L, Ghosh S, Wright CJ, Inhibition of IkappaBbeta/ NFkappaB signaling prevents LPS-induced IL1beta expression without increasing apoptosis in the developing mouse lung, *Pedia Res* 82 (6) (2017) 1064–1072.
- [45]. Turner MD, Nedjai B, Hurst T, Pennington DJ, Cytokines and chemokines: at the crossroads of cell signalling and inflammatory disease, *Biochim Biophys. Acta* 1843 (11) (2014) 2563–2582. [PubMed: 24892271]
- [46]. Jorda R, Hendrychova D, Voller J, Reznickova E, Gucky T, Krystof V, How selective are pharmacological inhibitors of cell-cycle-regulating cyclin-dependent kinases? *J. Med Chem* 61 (20) (2018) 9105–9120. [PubMed: 30234987]

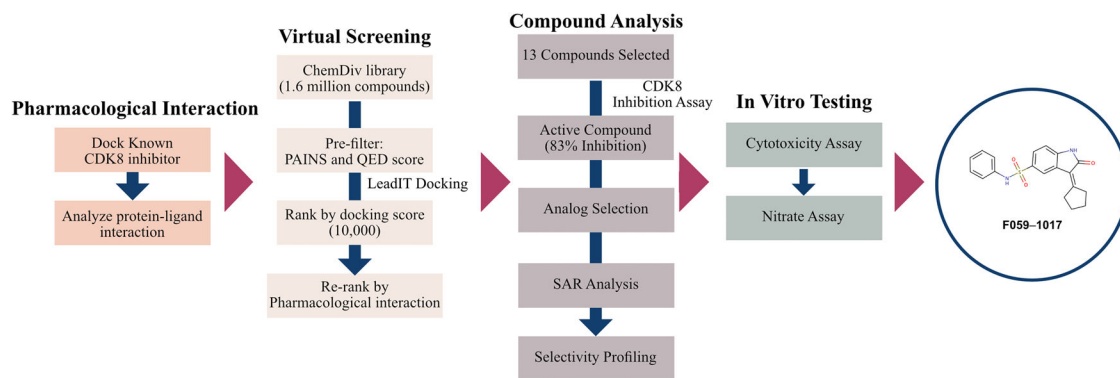


Fig. 1.
Schematic workflow of the study.

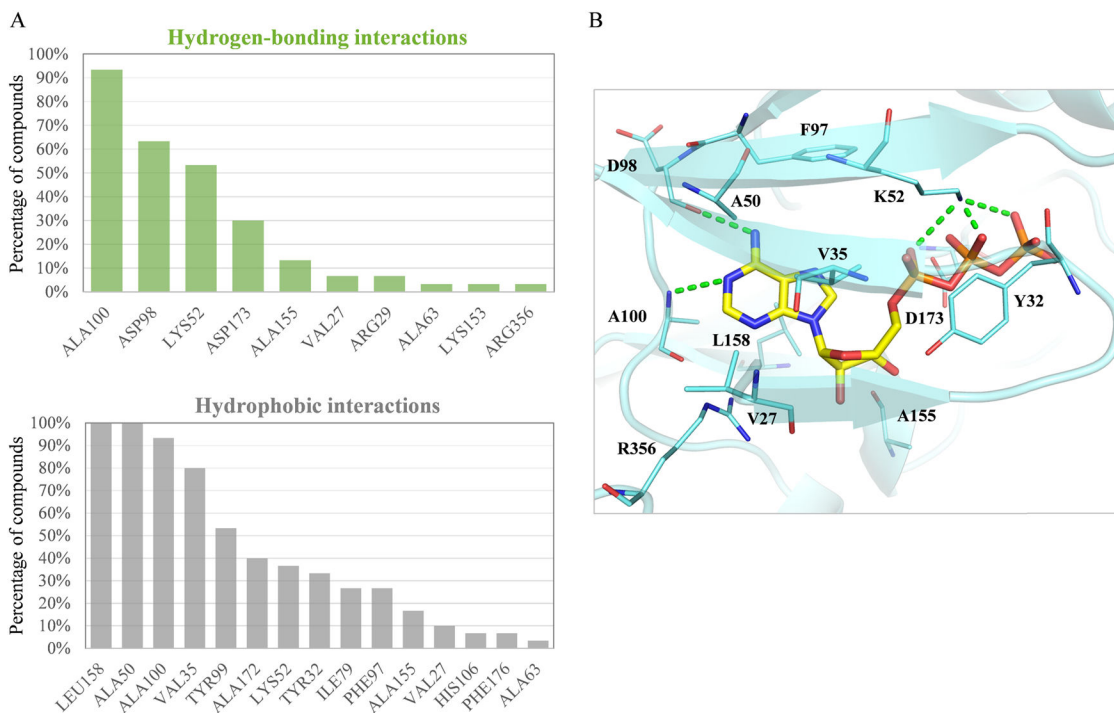


Fig. 2. Pharmacological interactions for CDK8. In total, 30 known CDK8 inhibitors with diverse structures were docked into the ATP binding site. (A) Frequency of hydrogen-bonding and hydrophobic interactions. (B) The binding pose of ATP in CDK8. The CDK8 (PDB ID: 5HBH) binding site is depicted in blue and ATP in yellow. Binding site residues are labeled shown. Hydrogen bonds are visualized as dashed green lines. (For interpretation of the references to colour in this figure legend, the reader is referred to the web version of this article.)

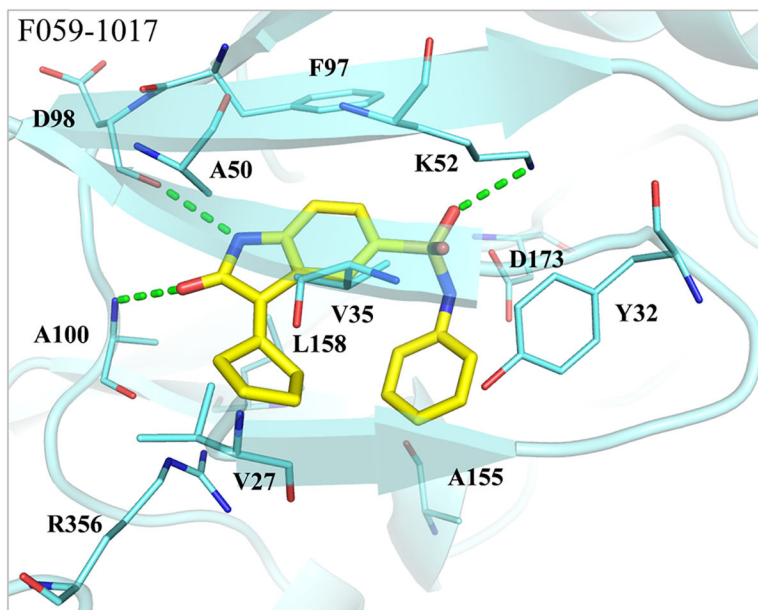


Fig. 3. Binding pose of the inhibitor. Compound F059–1017 (yellow) was docked into the CDK8 binding site (blue). Binding site residues are shown as sticks. Hydrogen bonds are visualized as dashed green lines. (For interpretation of the references to colour in this figure legend, the reader is referred to the web version of this article.)

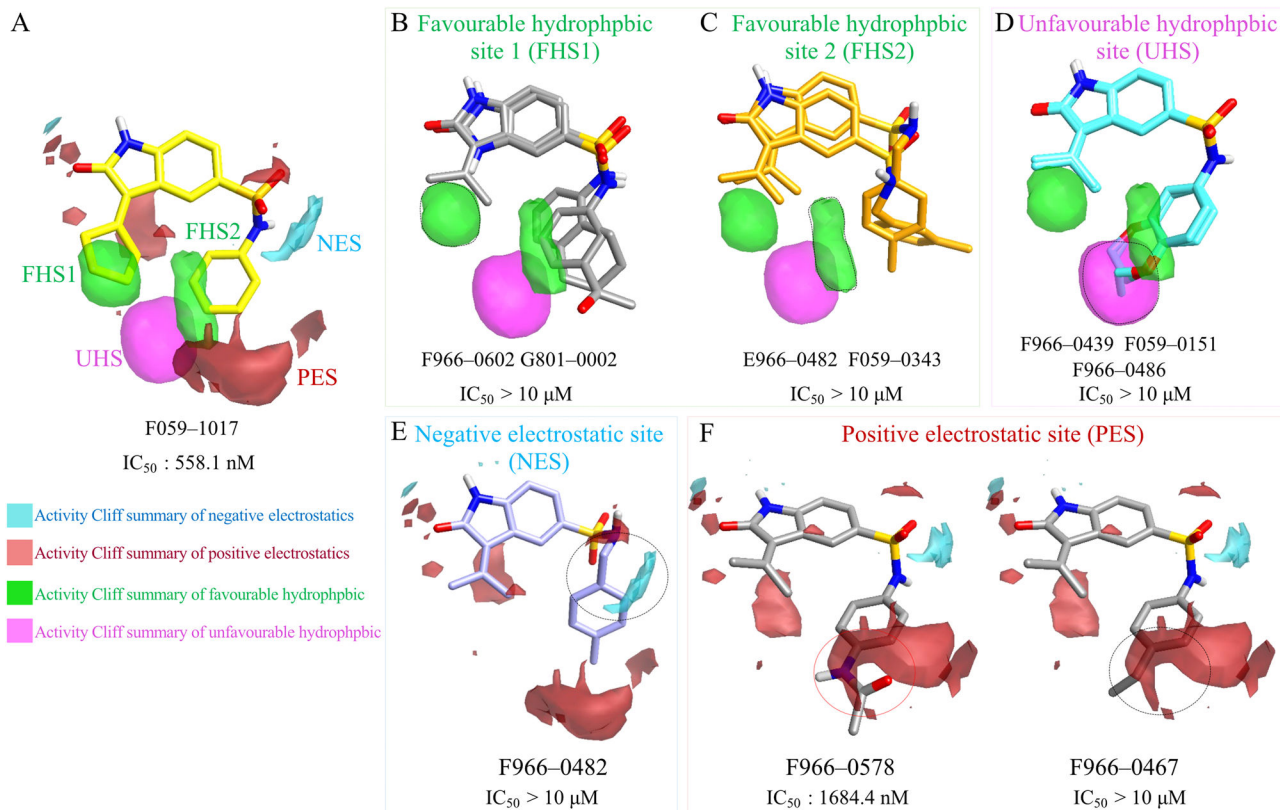


Fig. 4. Structure-activity relationship (SAR) analysis of F059-1017 and its inactive analogs. (A) The activity cliff suggests that F059-1017 is in a favorable position. (B-D) Hydrophobic pockets that are occupied by inactive analogs. (E, F) Inactive analogs have unfavorable electrostatic interactions.

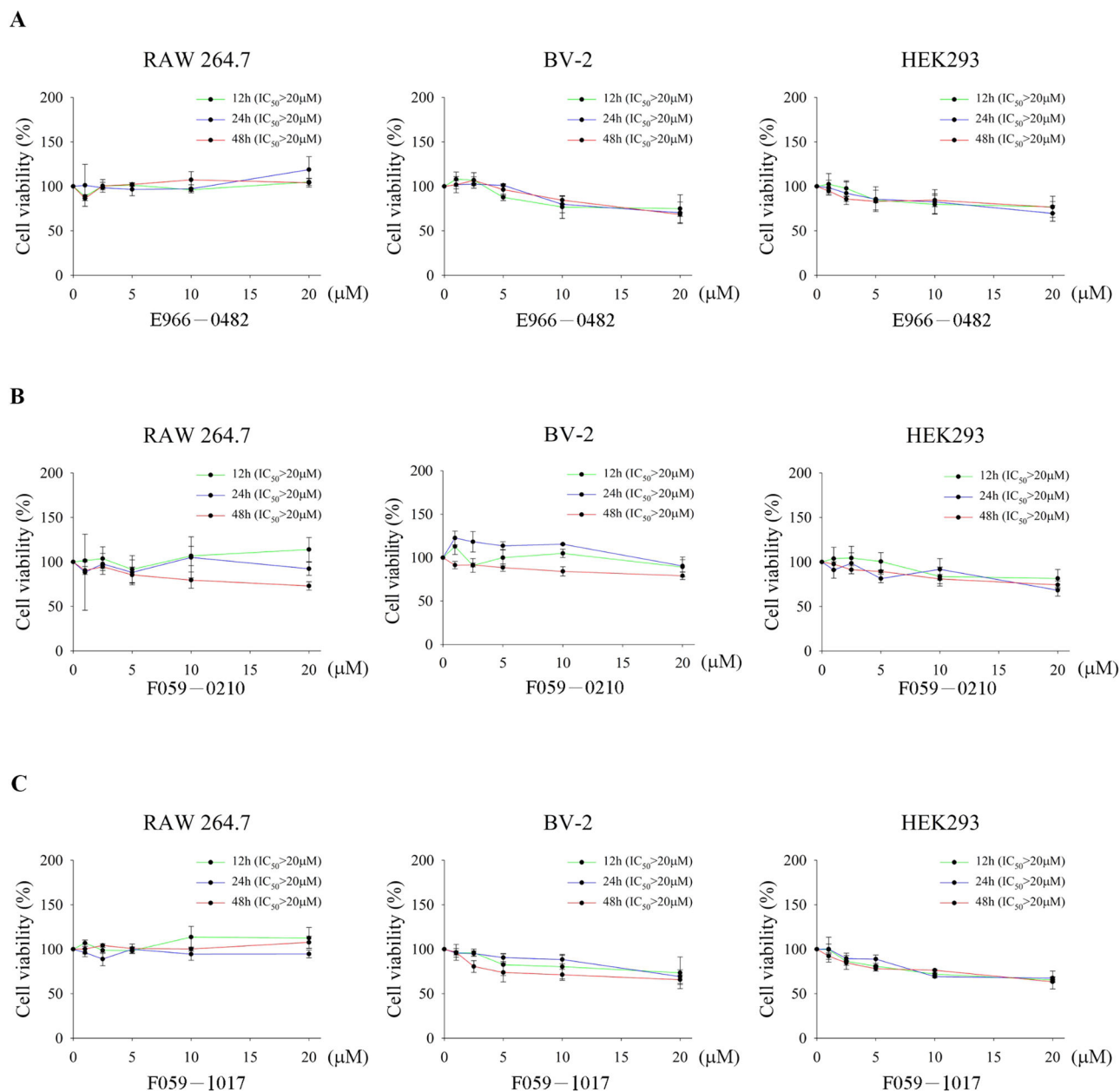


Fig. 5. Cell viability assay of test compounds. RAW264.7, BV-2, and HEK293 cells were incubated for 12, 24, or 48 h with or without the indicated concentrations of test compounds. Cell viabilities were determined by an MTT assay. Results are shown as the mean \pm SEM of three independent experiments.

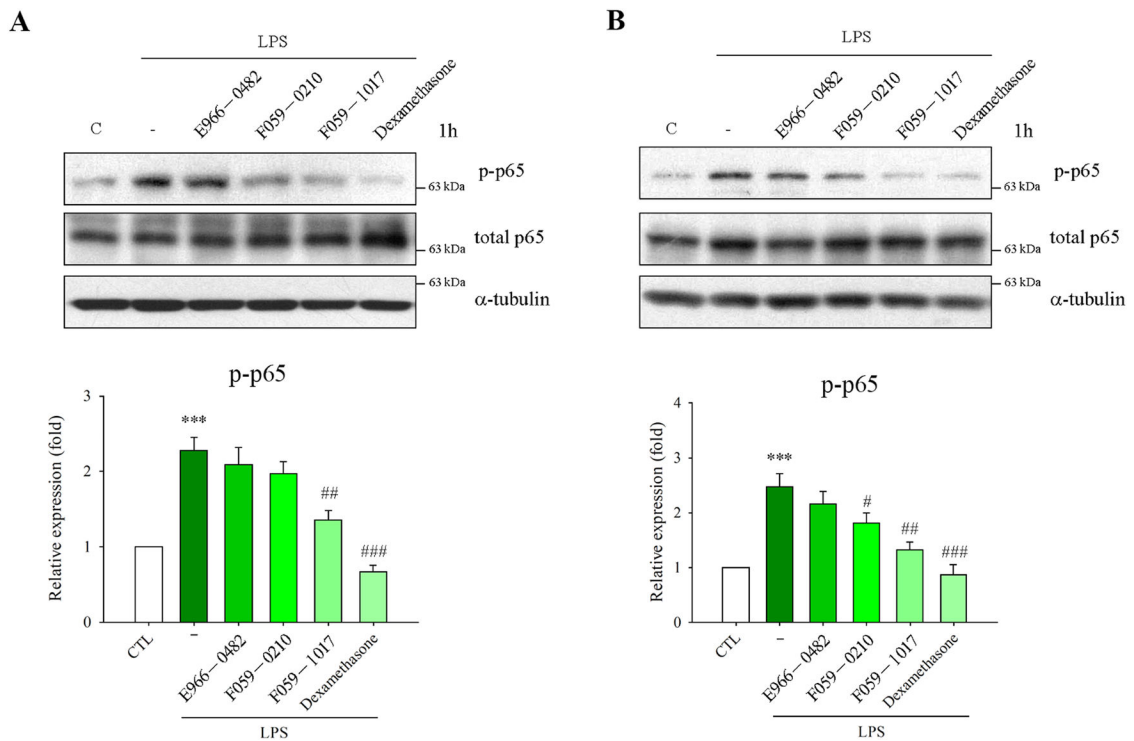
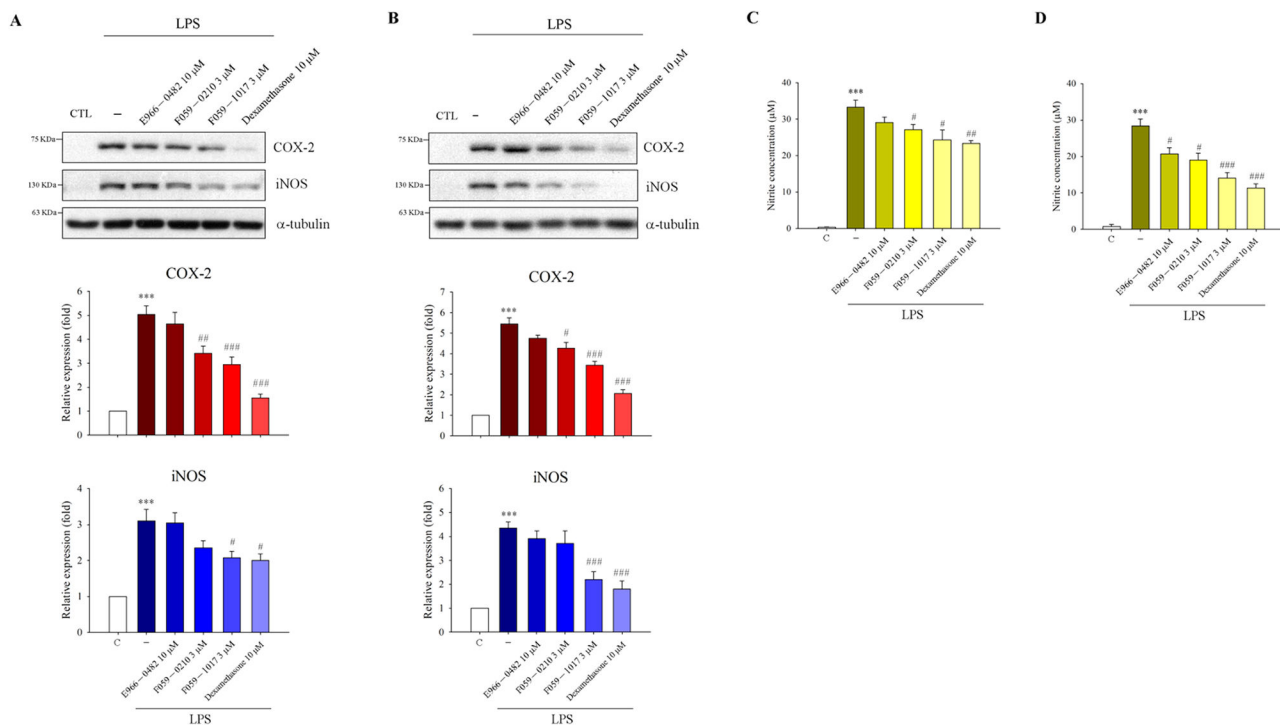


Fig. 6. Inhibition of phosphorylation of NF- κ B by CDK8 inhibitors in LPS-activated microglia and macrophages. (A) BV-2 and (B) RAW264.7 cells were treated with test compounds (10 μ M) or 10 μ M of dexamethasone for 1 h and stimulated with LPS (100 ng/mL) for an additional hour. Cell lysates were subjected to a Western blot analysis using the indicated antibodies. Results are shown as the mean \pm SEM from three independent experiments. * $p < 0.001$ compared to the control group; # $p < 0.05$, ## $p < 0.01$, and ### $p < 0.001$ compared to the LPS-treated group.

**Fig. 7.**

Inhibitory effect of CDK8 inhibitors on the inflammatory response. BV-2 (A, C) and RAW264.7 (B, D) cells were treated with test compounds at the indicated concentrations or 10 μ M dexamethasone for 1 h, followed by stimulation with LPS (100 ng/mL) for 24 h to induce COX-2 and iNOS expressions. Cell lysates were subjected to a Western blot analysis using the indicated antibodies (A, B), and supernatants were collected and assayed for nitrite (C, D). Results are shown as the mean \pm SEM from three independent experiments. * ** $p < 0.001$ compared to the control group; # $p < 0.05$, ## $p < 0.01$, and ### $p < 0.001$ compared to the LPS-treated group.

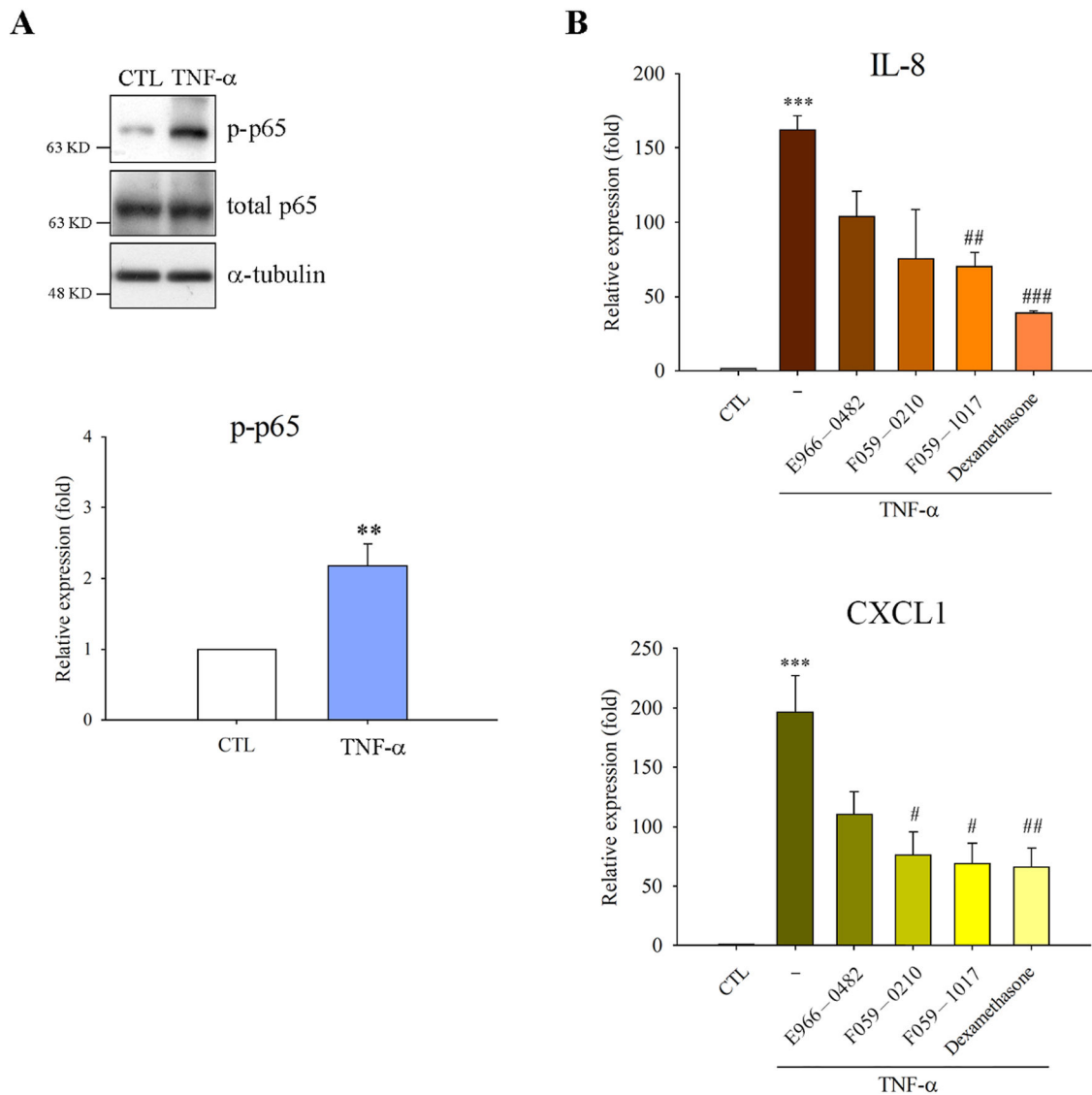


Fig. 8. CDK8 inhibition reduced expressions of pro-inflammatory mediators. HEK293 cells were incubated with test compounds (10 μ M) or 10 μ M dexamethasone for 1 h, followed by treatment with 10 ng/mL TNF- α for 2 h. (A) Cell lysates were subjected to a Western blot analysis using the indicated antibodies. (B) Relative expressions of IL-8 and CXCL1 were determined by a real-time PCR. * * $p < 0.01$ and * * * $p < 0.001$ compared to the control group; # $p < 0.05$, ## $p < 0.01$ and ### $p < 0.001$ compared to the TNF- α -treated group.

Table 1

Inhibitory activities of selected compounds.

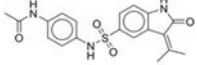
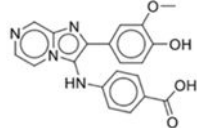
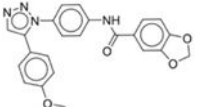
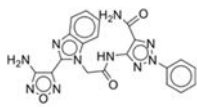
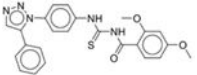
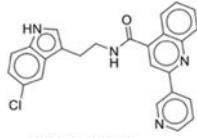
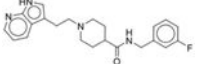
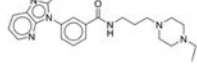
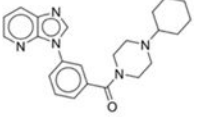
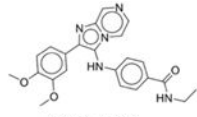
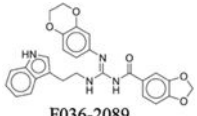
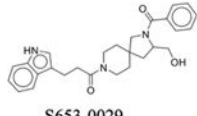
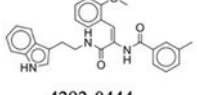
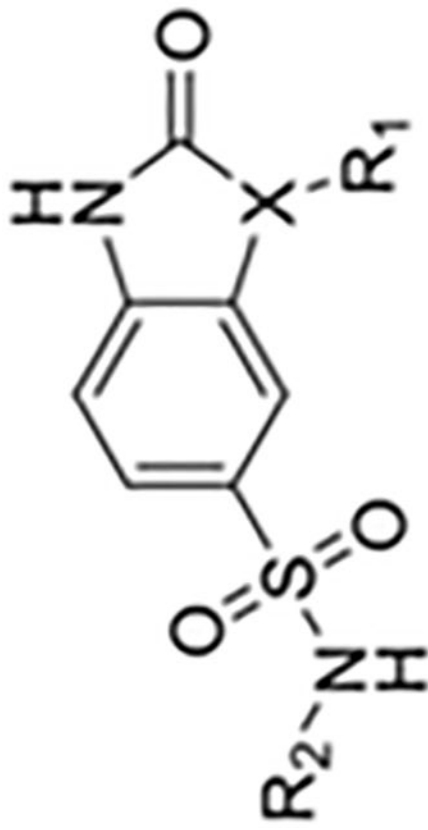
Compound	Inhibition percentage at 10 μ M	Compound	Inhibition percentage at 10 μ M
 E966-0578	83	 D401-0749	3
 K415-0170	48	 8012-7215	1
 K415-0366	27	 G547-0687	1
 M513-1938	26	 E760-5483	0
 E760-4964	16	 D401-0392	0
 F036-2089	4	 S653-0029	0
 4292-0444	3		

Table 2

Structures of selected analogs. The inhibitory activity is listed as shown.



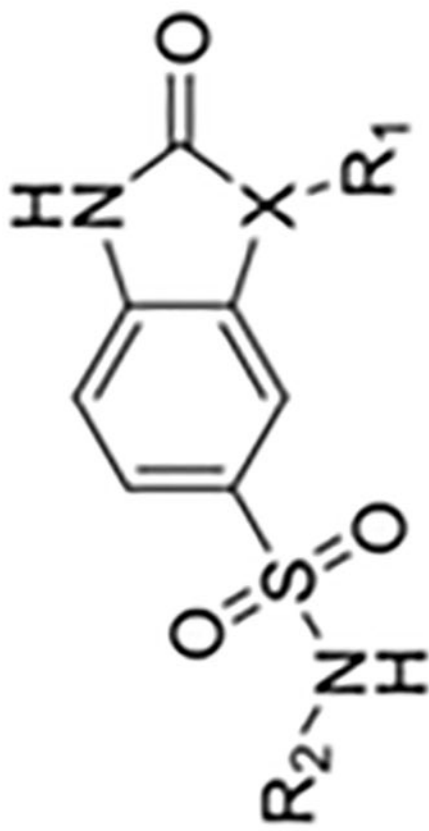
Compound	R ₁	R ₂	X	Inhibition percentage at 10 μM	Compound	R ₁	R ₂	X	Inhibition percentage at 10 μM
F059-1017			C	96	E966-0486			C	76
					E966-0529			C	39

Author Manuscript

Author Manuscript

Author Manuscript

Author Manuscript



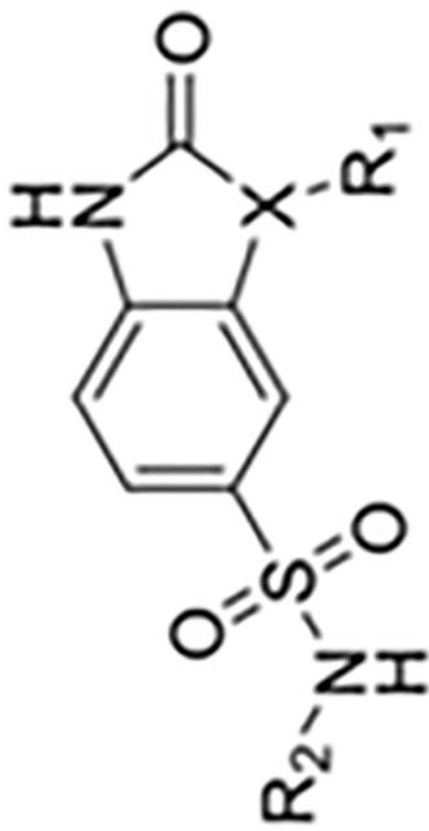
Compound	R ₁	R ₂	X	Inhibition percentage at 10 μM	Compound	R ₁	R ₂	X	Inhibition percentage at 10 μM
F059-0909			C	59	F059-0107			C	65
F059-0837			C	42	E966-0530			C	64
			C	37	E966-0602			C	37
			C	20	F059-0040			C	20

Author Manuscript

Author Manuscript

Author Manuscript

Author Manuscript



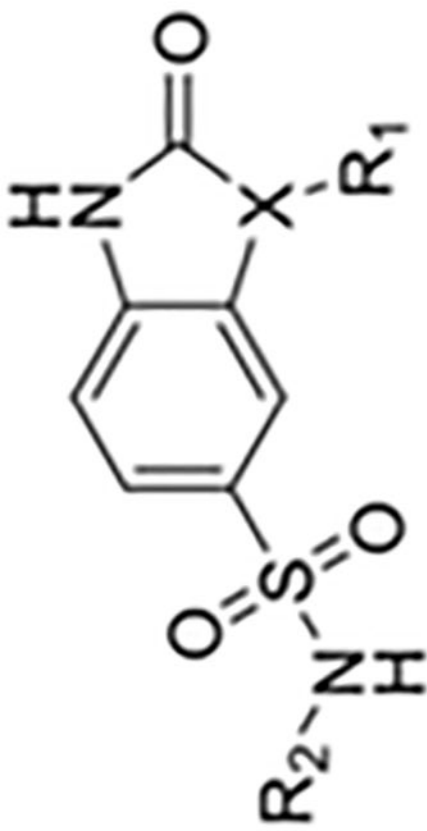
Compound	R ₁	R ₂	X	Inhibition percentage at 10 μM	Compound	R ₁	R ₂	X	Inhibition percentage at 10 μM
E966-0519			C	87	F059-0151			C	64
E966-0445			C	83	F059-0051			C	61
E966-0482			C	15	E966-0502			C	12

Author Manuscript

Author Manuscript

Author Manuscript

Author Manuscript



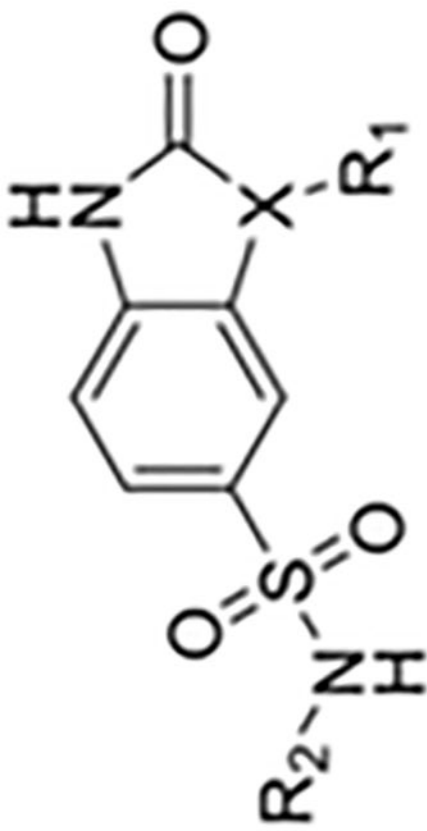
Compound	R ₁	R ₂	X	Inhibition percentage at 10 μM	Compound	R ₁	R ₂	X	Inhibition percentage at 10 μM
E966-0578			C	83	E966-0599			C	54
E966-0439			C	78	E966-0504			C	53
					F059-0343			C	8
					G801-0002			N	16

Author Manuscript

Author Manuscript

Author Manuscript

Author Manuscript



Compound	R ₁	R ₂	X	Inhibition percentage at 10 μM	Compound	R ₁	R ₂	X	Inhibition percentage at 10 μM
E966-0467				78	F059-0210				44

Table 3IC₅₀ values of selected compounds.

Compound	IC ₅₀ (nM)
F059-1017	558.1
E966-0530	1493.6
E966-0578	1684.4
E966-0445	2573

Author Manuscript

Author Manuscript

Author Manuscript

Author Manuscript